Linking Attentional States and Neuronal Dynamics in the Locus Coeruleus During a Decision-Making Task

A thesis
submitted towards the partial fullfilment of
the BS-MS dual degree programme
by

Ananya Joshi

Indian Institute of Science Education and Research Pune
Dr. Homi Bhabha Road,
Pashan, Pune 411008, INDIA

under the guidance of
Dr Matthias Prigge
Leibniz Institute for Neurobiology
Magdeburg, Germany

from June 2024 to March 2025

Certificate

This is to certify that this dissertation entitled **Linking Attentional States and Neuronal Dynamics in the Locus Coeruleus During a Decision-Making Task** submitted towards the partial fulfillment of the BS-MS dual degree programme at the Indian Institute of Science Education and Research, Pune represents original research carried out by Ananya Joshi at Leibniz Institute for Neurobiology, under the supervision of Dr Matthias Prigge during the academic year 2024-2025.

Thesis Advisory Committee

Supervisor
Dr Matthias Prigge

Expert
Dr Nixon Abraham

Declaration

I, hereby declare that the matter embodied in the report titled **Linking Attentional States and Neuronal Dynamics in the Locus Coeruleus During a Decision-Making Task** is the result of the investigations carried out by me at the Leibniz Institute for Neurobiology from the period 01-06-2024 to 31-03-2025 under the supervision of Dr Matthias Prigge and the same has not been submitted elsewhere for any other degree.

Ananya Joshi
Roll number: 20201034
BS-MS
IISER Pune
Date: 31/03/2025

Dedicated to my mother, Lalita

Acknowledgements

I sincerely thank my supervisor, Dr Matthias Prigge, for allowing me to work on this project and providing me with support and resources throughout the project. I am incredibly grateful to Csilla Novák for teaching me everything in the lab and being a constant pillar of support. I thank Vera Evander for getting me started recording and analysing fibre photometry. I thank Csilla Novák and Rukhshona Kayumova for performing stereotactic surgeries for this project. I thank Susmita Das, Sama Ghani, Diana Munnicchi and Rukhshona Kayumova for helping with immunohistochemistry. I want to thank all members of the Neuromodulatory Networks group for their constant help and support.

I am grateful for the support and resources provided by the Leibniz Institute of Neurobiology during this project. I want to thank the International Brain Laboratory community for helpful discussions on the mice behavioural task.

I thank my expert, Dr Nixon Abraham, for valuable discussions on this project. I am also grateful to him and the Laboratory of Neural Circuits and Behaviour for introducing me to mice behaviour and neurobiology.

I am grateful to IISER, Pune, for providing a rich environment to help me navigate my research journey. I acknowledge Innovation in Science Pursuit for Inspired Research (INSPIRE), DST, Government of India for the scholarship.

I am immensely grateful to my mother for always being my biggest supporter. Lastly, I want to thank all my teachers.

Contributions

Contributor name	Contributor role
A. Joshi, C. Novák, M. Prigge	Conceptualization of Ideas
A. Joshi, C. Novák, S. Kayumova	Methodology
A. Joshi	Software
M. Prigge	Validation
A. Joshi	Formal analysis
A. Joshi	Investigation
M. Prigge	Resources
A. Joshi	Data Curation
A. Joshi	Writing — original draft preparation
C. Novák, M. Prigge	Writing — review and editing
A. Joshi,	Visualization
M. Prigge	Supervision
M. Prigge	Project administration
M. Prigge	Funding acquisition

Abstract

Our brains perform a remarkable number of computations continuously to interpret our external environments and respond appropriately. While performing a cognitive task, we may direct attention to the stimuli specific to the current task, alternative stimuli in the environment, past knowledge and experiences, or our internal biases when making decisions. This selective attention is an essential property of our brains, allowing the allocation of cognitive resources to relevant information, filtering out distractions and optimising cognitive performance. Locus coeruleus, the primary noradrenaline (NA) releasing brainstem nucleus, impacts diverse cognitive functions like attention, arousal, sensory processing and goal-directed behaviour (Poe et al., 2020). The LC is also a vulnerable brain structure, being one of the first areas that undergo degeneration during the pathology of neurodegenerative diseases such as Parkinson's and Alzheimer's. Additionally, while the early-stage symptoms of these diseases can be variable, they often affect attention (Muslimovic, Post, Speelman et al, 2005; Sharpe, 1992). However, the complete role of the LC-NA network in attention during health and disease remains elusive. In this study, we modelled attentional states exhibited by mice during a vision-based perceptual decision-making task (International Brain Laboratory et al., 2021) using a Bernoulli generalised linear model - hidden Markov model (GLM-HMM: Ashwood et al., 2022). Each identified attentional state has a different dependency on variables like task-relevant stimuli, internal bias, and history, such as previous response and reward, describing degrees of engagement. We explored the calcium dynamics of LC neurons during these attentional states through fibre photometry. We found that the mean calcium activity of the LC neurons just after stimulus presentation seems to predict the attentional state of mice during this task and, thus, the related accuracy/performance and task-relevant stimulus sensitivity. This framework, presented here, sets the groundwork for predicting task engagement and performance from LC activity.

Contents

List of Figures

List of Tables

Chapter 1

Introduction

Information transfer in our brains is facilitated by chemical messengers called neurotransmitters. They travel across a synapse and act on post-synaptic cells by binding to specific receptors. These neurotransmitters can be classified as excitatory (glutamate), inhibitory (GABA) or neuromodulatory based on how they affect the post-synaptic cells through their receptors (Slater et al., 2022). In addition to being excitatory and inhibitory, neuromodulators can influence a wide range of effects on neuron populations, such as modulating the degree of this excitation/inhibition and the effects of other neurotransmitters. These neuromodulators primarily act through G-protein coupled receptors modulating neuronal excitability and synaptic plasticity. Neuromodulatory circuits have a highly distributed axonal network throughout the central nervous system. These networks are capable of differentially influencing information processing for cognitive functions through distinct sub-system projections in the cortex (Zaborszky, 2004; Golmayo et al., 2003; Slater et al., 2022; Poe, Foote, Eschenko et al., 2020).

Noradrenaline (NA) is one of the primary neuromodulators released in our brains. It is highly evolutionarily conserved. It affects various cognitive functions such as arousal, attention, sensory processing, plasticity, memory formation, stress, behavioural flexibility, motivation and decision-making, but the mode of action is a matter of active research (Poe, G.R., Foote, S., Eschenko, O. et al., 2020). Locus coeruleus (LC) is the largest group of noradrenaline-releasing cells among other smaller neuron groups distributed in the pons and medulla region of the brain stem (Robertson et al., 2013). It is a small bilateral pair of nuclei in the brainstem consisting of around 3000 neurons in the rodent brain (Sara, 2009). It provides the primary source of noradrenaline for the neocortex, hippocampus, amygdala, thalamus and cerebellum (Lindvaal & Bjorklund, 1974). LC-NA neurons also exhibit particular sensitivity to pathology and mortality in age-related neurodegenerative dis-

eases (Poe, Foote, Eschenko et al., 2020). In Alzheimer's disease (AD), LC is among the first brain regions to show the appearance of hyperphosphorylated 'pretangle' tau pathology. They are among the first structures affected by α-synuclein inclusions in Parkinson's disease (PD). These neurodegenerative diseases also involve deficits in attentional focus in the early stages. In the later stages of both AD and PD, LC cell loss becomes catastrophic (Poe, Foote, Eschenko et al., 2020).

Decoding the complex role of this neuromodulator in higher cognitive behaviours is essential for predicting normal brain functions and addressing early detection and treatment options for neurological disorders. In this thesis, we study the role of the neuromodulator noradrenaline during a perceptual decision-making task in mice through calcium activity in the locus coeruleus neurons.

1.1 LC circuitry

The locus coeruleus projects to multiple cortical regions, such as the prefrontal, orbitofrontal, medial prefrontal, anterior cingulate, and motor cortices (Pickel, Segal, and Bloom, 1974; Jones & Moore, 1977) that are crucial in the modulation of attention, arousal, and cognitive functions. It innervates limbic structures, influencing memory formation, emotional processing, and stress responses (McCall et al., 2017; Benarroch, 2018). It also has extensive connections to thalamic and hypothalamic structures, which are implicated in sensory processing, arousal, and homeostatic functions (Ginsberg et al., 1993; Aston-Jones & Cohen, 2005; Benarroch, 2018). Projections from the LC to the brainstem nuclei and spinal cord play a role in pain modulation (Hickey et al., 2014; Westlund & Coulter, 1980; Benarroch, 2018). These projections exhibit varying densities throughout the brain, notably high concentrations in the cortex and hippocampus. They also arise from distinct spatially organised cells in the locus coeruleus (Loughlin, Foote, and Bloom, 1986; Benarroch, 2018). The LC receives afferent inputs from the forebrain regions, brainstem areas, and the cerebellum. The forebrain afferents release molecules such as glutamate (Arnsten & Goldman-Rakic, 1984), corticotrophin-releasing hormone (Pammer et al., 1990), and hypocretin/orexin (Downs et al., 2007), which impact cognitive function, arousal states, emotional processing, stress responses, and homeostatic functions (Benarroch, 2018). It also receives nociceptive inputs from the spinal cord (Westlund & Craig, 1996).

Noradrenaline influences its targets via G-protein coupled receptors, specifically $\alpha 1$, $\alpha 2$, and β receptors (Benarroch, 2018). The $\alpha 1$ receptors are ma-

jorly found post-synaptically and promote excitatory effects. While the $\alpha 2$ receptors are situated at both pre-synaptic and post-synaptic locations. They inhibit neuronal excitability and release of neurotransmitters. The β receptors are found post-synaptically and influence cell excitability and plasticity (Benarroch, 2018).

1.2 LC-NA activity and Behaviour

Neurons generally exhibit different firing patterns. Regular, low-frequency baseline firing is called tonic activity, while high-frequency bursts in response to specific stimuli are called phasic firing. These firing patterns are associated with behavioural states in the LC. Tonic firing at 1 to 5 Hz is associated with arousal states, while phasic firing, consisting of two to three spikes at 10 to 20 Hz, occurs after salient stimuli or focused attentional tasks (Aston-Jones & Cohen, 2005). Multiple theories/ models try to elucidate the role of LC-NA neurons in behaviour.

During periods of high-performance accuracy, phasic LC responses are observed during moderate tonic firing after the target stimuli presentation (Aston-Jones & Cohen, 2005). These responses are not specific to sensory attributes, rewards, or target values. This phasic activity occurs before behavioural responses and is thought to be influenced by the results of "internal decision-making processes" (Aston-Jones & Cohen, 2005). During a signal detection task, LC phasic responses in monkeys were shown to have a very short rise time of 100 ms and preceded the responses by 200 ms (Aston-Jones et al., 1994). On the other hand, high levels of LC tonic activity correlated with decreased performance and disengagement. According to the Adaptive Gain theory (Aston-Jones & Cohen, 2005), phasic LC activity facilitates behavioural responses during task-related decision-making processes, while the lack of LC phasic activity allows the animal to disengage from the task. This theory indicates that rapid tonic activity is crucial for exploring alternative strategies and adaptive behaviour in a dynamic environment.

The Adaptive Gain model (Aston-Jones & Cohen, 2005) compares decision processes to basic accumulators that integrate signals supporting each choice option as neural gain and conclude when the difference between these options crosses a threshold value. This model suggests that the LC responds phasically during decision-making when the neural gain of any unit related to a choice crosses the threshold. This phasic response increases the neural gain across all units in the behavioural network, preventing additional signal integration. This ensures that the last signal that crossed threshold affects the behavioural response. The LC-NA signal is a global signal that adapts

neural circuits by modulating neural gain to enhance selective attention and performance (Aston-Jones & Cohen, 2005). According to this hypothesis, LC phasic responses during low tonic (baseline) activity result in adaptive changes in neuronal gain, maximising performance on a given task. Conversely, elevated LC tonic activity consistently enhances neural gain across all units, increasing the system's sensitivity to stimuli.

In recent years, there has been more evidence for this theory (Maness et al., 2022). The phasic LC-NA response is essential for attention-related gamma oscillations in the prefrontal cortex triggered by foot shocks (Neves et al., 2018). Tonic optogenetic stimulation of LC-NA neurons resulted in prolonged alertness and amplified high-frequency and diminished low-frequency cortical oscillations (Dahl et al., 2022; Marzo et al., 2014). Moderate NA activity during an auditory signal detection task was associated with optimal performance. Too low/high cortical activation through NA reduced task performance (Dahl et al., 2022).

The Network Reset theory (Bouret & Sara, 2005) is another theory that discusses the relationship between LC-NE activity and behaviour. This theory is derived from an invertebrate model. Depending on the system's state, a single neuron may engage in different networks in crustaceans. Also, a single anatomical network may carry out different functions. Synchronous input from neuromodulatory cells can suddenly disrupt activity in these brain networks and reorganise the components into different functional networks. G-protein coupled receptors mediate this effect by influencing cellular excitability and synaptic strengths. This "global reset function" of neuromodulatory systems in invertebrates is proposed to be similar to NA in vertebrates (Bouret & Sara, 2005). In mammals, "the phasic activation of noradrenaline-releasing neurons in the locus coeruleus, synchronised with cognitive shifts, may promote the dynamic reorganisation of target neural networks, facilitating rapid behavioural adaptation". Simultaneous multi-electrode recordings from the LC and forebrain regions during an olfactory go/no-go task demonstrated that LC responses precede those in the forebrain, both intra- and inter-trial, supporting the role of LC activation as a reset signal that facilitates cognitive shifts (Bouret & Sara, 2005). LC neurons are activated in behavioural conditions involving cognitive transitions, such as interrupting ongoing actions and adaptative behaviour. In go/no-go trials involving rats, diminished LC activity was observed during active attention on the task, inhibiting behavioural changes and distractions from irrelevant stimuli (Bouret & Sara, 2005). This theory argues that LC activity is unrelated to decision-making or reward anticipation, as there is no evidence of LC activation before the behavioural reaction and a reduction in firing rate was observed during the 600 ms interval when the animal was executing a response before the

reward. During trials, LC neurons were activated by events involving behavioural modifications, such as a start signal, target stimuli, or anticipated rewards (Bouret & Sara, 2005).

Another contemporary model, the unexpected uncertainty model by Yu & Dayan (2005), proposes that NA plays a role in balancing bottom-up sensory processing and top-down interpretations. It proposes that NA signals "unexpected uncertainty" within a behavioural context indicating a discrepancy between predictions and observations. Thus, the LC-NA network promotes learning and adaptation to dramatic changes. A recent corollary to this model, the LC global failure model, proposes that LC communicates "unsigned prediction errors" (Rebecca Jordan, 2023). These signals do not depend on the valence (aversive/rewarding) of the error, that is, whenever there is a difference between the learned internal assumptions about the sensory input and the actual sensory input received. During a visuomotor learning task, the LC responses scaled with the size of the visuomotor error (Jordan & Keller, 2023). It proposes that this error prediction signal from the LC regulates the balance between top-down predictions and bottom-up sensation, promoting adaptive behaviour through corrective learning and plasticity.

These theories are not mutually exclusive; however, none can fully elucidate the role of LC-NA in the brain. In recent years, minimal advances have been made in refining or unifying these elements.

1.3 Thesis Overview

Here, we have investigated attentional states and LC-NA neuronal activity in mice engaged in a vision-based perceptual decision-making task (International Brain Laboratory et al., 2021). The mouse is presented with a visual stimulus on a screen. This stimulus can appear on the screen's right or left, and the mouse has to learn to move a wheel in the opposite direction to bring the stimulus to the centre. The mouse is rewarded with sweet water on correct trials, and a noise burst follows incorrect trials or omissions. The attentional states are identified as decision-making strategies adopted by the mice during this task, reflecting the varying dependence of the mouse's responses on stimuli, internal biases, and prior history, including past choice and reward, through the application of a probabilistic model (GLM-HMM; Ashwood et al., 2022). This model consists of a hidden Markov model (HMM) with hidden states defined by Bernoulli generalised linear models (GLMs). States with highly stimulus-dependent responses represent 'engaged' states, while the' disengaged' states exhibit weak stimuli dependence or biased choices. We discovered that expert mice adopt different attentional states during a

session using a 3-state GLM-HMM model similar to Ashwood et al. (2020). We also used fibre-photometry to examine the LC-NA neuronal activity during these latent attentional states.

Chapter 2

Methods

2.1 Experimental animals

All experiments and procedures are conducted strictly under the guidelines of the EU Council Directive 2010/63/EU, the German Animal Welfare Act (Tierschutzgesetz), and are approved by the local Committee for Ethics and Animal Research (Landesverwaltungsamt Sachsen-Anhalt, Germany) (42502-2-1715 LIN). Mice from C57BL/6J (JAX ID: 000664), DBH-cre (JAX ID: 033951), TH-cre (JAX ID: 008601) and DH-cre × hTyr x Ai9 (JAX ID: 007905) strains are used for the study. All mice are 9–12 weeks old at the time of the surgery and are co-housed whenever possible. The mice are kept on a 12-hour light/dark cycle, and experiments are performed during the light cycle.

2.2 Surgery

All surgical procedures are conducted under inhalation anaesthesia — 3.5% isoflurane for induction and 1.5–2% isoflurane for maintenance. The mice are head-fixed on a stereotaxic device. The fur is shaved, the scalp is disinfected with 20% ethanol, and Lidocaine is applied. A small incision is made on the scalp along the anterior/posterior axis to expose the bregma and lambda, and the head is levelled along the anterior/posterior (A/P), medial/lateral (M/L) and dorsal/ventral (D/V) axes. The skull is cleaned and disinfected with H2O2. After identification and alignment of the bregma and lambda, a hole is drilled through the skull at the injection and implant sites. A viral suspension (cre-dependent GCaMP8f: AAV-shortCAG-dlox-jGCaMP8f(rev)-dlox-WPRE-SV40p(A), non-cre-dependent GCaMP8f: AAV-Syn-jGCaMP8f-WPRE) is slowly injected at the LC coordinates with

Group	Number of mice	Virus	Injection site (wrt bregma)	Injection rate	Implant site (wrt bregma)
DBH-cre	7 ♂	Cre-dependent GCaMP8f	-5.4 A/P, 1-1.1 M/L, -3.5 D/V	700 nl at 75 nl/min	-5.34 A/P, 2.24 M/L, -3.12 D/V at 20°/20° angle caudal/lateral
DBH x Ai9	1 ♂	Cre-dependent GCaMP8f	-5.4 A/P, 1 M/L, -3.5 D/V	700 nl at 75 nl/min	-5.34 A/P, 2.24 M/L, -3.12 D/V at 20°/20° angle caudal/lateral
TH-cre	7 ♂+2 ♀	Cre-dependent GCaMP8f	-(5.35-5.4) A/P, 1.1-1.2 M/L, -(3.5-3.6) D/V	700 nl at 75 nl/min	-5.34 A/P, 2.24 M/L, -3.12 D/V at 20°/20° angle caudal/lateral
WT control (C57BL/6J)	3 ♂	Cre-dependent GCaMP8f	-(5.35-5.4) A/P, 1.1-1.2 M/L, -(3.5-3.6) D/V	700 nl at 75 nl/min	-5.34 A/P, 2.24 M/L, -3.12 D/V at 20°/20° angle caudal/lateral
WT experimental (C57BL/6J)	4 ♂	Non-cre-dependent GCaMP	-(5.35-5.4) A/P, 1.1-1.2 M/L, -(3.5-3.6) D/V	600 nl at 50 nl/min	-5.34 A/P, 2.24 M/L, -3.12 D/V at 20°/20° angle caudal/lateral

Table 2.1: Details of stereotactic surgery in mice

a 34 G bevelled needle or a glass pipette. The needle is withdrawn slowly at 0.01 mm/s after 10 minutes. The optical fibre implant (400 µm diameter/4.5 mm length) is placed with a similar approach above the LC. After applying a dental primer, the implant is secured to the skull using Plurafill Flow+. Then, the head plate is placed on the skull and secured with Plurafill Flow+ (as per International Brain Laboratory (2022). Appendix 3: IBL protocol for craniotomy surgery). The implants are secured with dental acrylic cement, and the incision is closed with sutures if required. Post-surgery, the animals are monitored and given pain medication (carprofen) for three days.

2.3 Behavioural Task

2.3.1 Water restriction

The mice are given water ad libitum for two weeks post-surgery during recovery. From the third week onwards, the mice are given 1.5–2% citric acid solution in their home cages as an alternative for total water restriction. The body weight is monitored throughout to ensure it stays above 87% of the baseline weight measured before the start of water restriction. If the body weight drops below this, the mice are given ad libitum water in their home cages.

2.3.2 Habituation

We follow a standardised perceptual decision-making paradigm (International Brain Laboratory et al., 2021). Post-surgery, the mice are handled for 10 minutes each day during recovery. The habituation to the rig starts from the second week onwards. The behaviour rig/set-up consists of a platform on which the mouse is head-restrained. A screen is placed in front of this platform such that the mouse's field of vision is centred. There is a wheel near the front of the platform where the front paws of the mouse are placed. A lick tube connected to the reward delivery system is placed near the snout to allow easy access to the reward. Three cameras record the body, the left and the right pupil, while a speaker plays the start cue at the beginning of each trial, and a noise burst following incorrect responses (International Brain Laboratory et al., 2021). In the habituation protocol, the visual stimulus (Gabor patch at 100% contrast) is presented on either of the two sides (right/left) of the screen. After an average of 10 seconds, the stimulus moves to the centre of the screen. This is followed by a drop of 10% sucrose solution (reward) through a tube after 500 ms. The stimulus

stays in the centre of the screen for another 500 ms, followed by an inter-trial interval of an average of 1 second. This trial cycle is repeated throughout the duration of the habituation session. On the first habituation day, the mice can freely explore the behavioural rig for 10 minutes. On the second day, the mice are head-fixed with the wheel-locked for 15-20 minutes during habituation protocol. On the third and the fourth day, the head-fixation time is increased to 30 and 60 minutes, respectively. The mice are immediately removed from the head restraint if there are any signs of stress. Refer to Appendix 2: International Brain Laboratory et al., 2021 for more details on the protocol.

2.3.3 Training

For training protocol, we follow Appendix 2: International Brain Laboratory et al., 2021. During the training period, the wheel is unlocked. For a trial to begin, the mouse must not move the wheel for a quiescence period of 400-700 ms. The timer is reset to zero if the wheel moves during this period. After this, the visual stimulus appears on the screen's right or left with equal probability and a start cue of 100 ms is played. The mouse has 60 seconds to move the Gabor patch to the centre of the screen by moving the wheel. The mouse receives the reward (10% sucrose solution) if it does a correct trial. The trial is marked as incorrect if the mouse moves the Gabor patch more than 35 degrees towards the opposite side. If the mouse fails to do either in 60 seconds, the trial is marked as a time-out. Time-out and incorrect trials end with a noise burst for half a second. After the reward/noise burst, a new trial starts following an inter-trial interval (1 s after a rewarded trial, 2 s after an incorrect/time-out trial).

The visual stimulus can be of different contrasts in each trial (Appendix 2: International Brain Laboratory et al., 2021). These contrasts are randomly selected from a set of contrasts, following a uniform distribution. Initially, this set has two contrasts — 100% and 50%. In further stages of the training, additional lower contrasts are added/removed to the contrast set. The different stages are described in the table below.

Before the 6th stage, if the mouse's response is incorrect for stimuli with more than 50% contrasts, the previous stimulus contrast is repeated, and the side of the stimulus is not randomly selected. The probability of the visual stimulus appearing on the same side as the incorrect trial increases. This is a soft counter-biasing to ensure that if the mouse is biased to move the wheel on one side, it is more likely that the correct movement in the following trials will be to the opposite side, and the trial will be registered as incorrect. An average session is run for 45 minutes if the mouse does less than 400 trials.

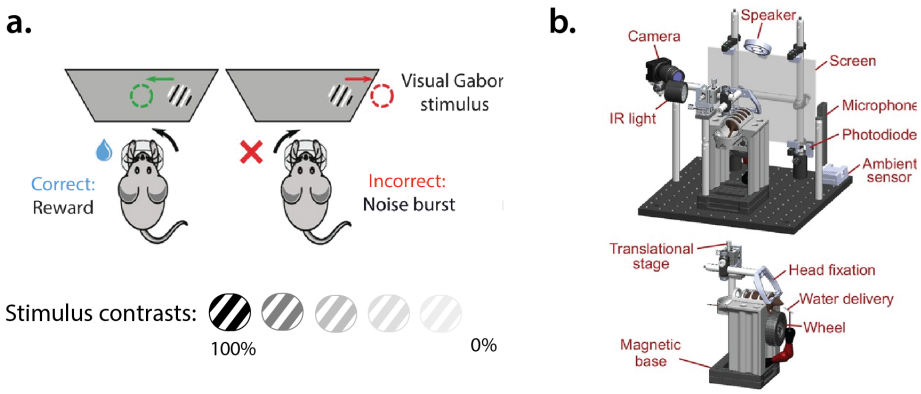

Figure 2.1: International Brain Laboratory et al. (2021) behavioural task in mice. **a.** A schematic of the task; **b.** A schematic of the set-up.

Stage	Stimuli contrasts	Criteria for progress
1	[50%, 100%]	$>$ 80% correct trials at each contrast
2	[25%, 50%, 100%]	$>$ 80% correct trials at each contrast
3	[12.5%, 25%, 50%, 100%]	$>$ 200 trials performed
4	[6%, 12.5%, 25%, 50%, 100%]	$>$ 200 trials performed
5	[0%, 6%, 12.5%, 25%, 50%, 100%]	$>$ 200 trials performed
6	[0%, 6%, 12.5%, 25%, 100%]	

Table 2.2: Training stages in the behavioural task

If the mouse does more than 400 trials in a session, the session is stopped if the mouse has been training for >45 minutes and has performed fewer than 45 trials in the last 5 mins. If a mouse fails to reach the last stage by training day 40, the mouse may be removed from the pipeline and labelled as untrainable. Refer to Appendix 2: International Brain Laboratory et al., 2021 for more details on the protocol.

2.3.4 Psychometric curve analysis

Psychometric plots are used to interpret mice behaviour during the perceptual decision-making task. This function models the dependence of the probability of making a rightward choice on the stimulus contrasts. To obtain a psychometric curve, data is fit with the following parametric error function,

using maximum likelihood algorithm.

$$P = \gamma + (1 - \gamma - \lambda) \cdot \frac{\text{erf}\left(\frac{c-\mu}{\Sigma} + 1\right)}{2}$$

Here, P is the probability of a rightward wheel turn response and c is the stimulus contrast. μ is the response bias, Σ is the contrast threshold, γ and λ refer to the low and high lapse rates respectively. μ, Σ, γ and λ are learned parameters. Response bias, μ, represents systemic bias towards choosing a particular side, while contrast threshold, Σ, describes sensitivity to stimuli contrasts. Smaller contrast thresholds denote high sensitivity to even low contrasts. High lapse rates, γ and λ, denote the failure of mice to respond correctly even at higher contrasts.

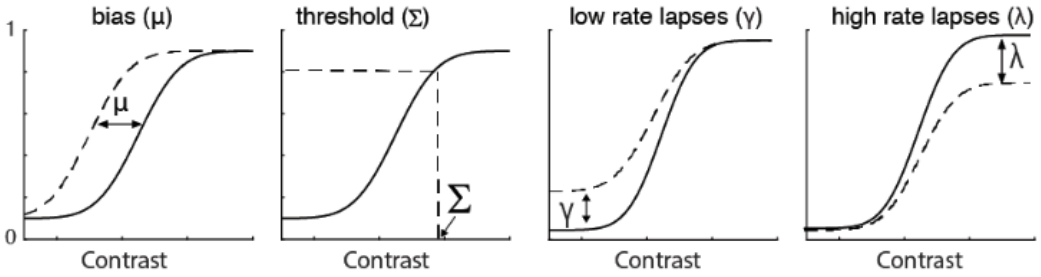

Figure 2.2: Psychometric curve parameters (Appendix 2: International Brain Laboratory et al., 2021)

2.4 GLM-HMM

2.4.1 Model fitting

We use the Bernoulli generalised linear model - hidden Markov model described in Ashwood et al., 2022 to identify decision-making strategies used by mice during the IBL training task. The GLM-HMM specifies a fixed number of latent states displaying varying dependence on the stimulus and other covariates during training sessions. There are two components in this model: an HMM and state-specific GLMs. Each GLM describes the decision-making strategy used in that state. The HMM part of this model determines the probabilities of transitioning between latent states with a K×K transition matrix (A). This can be represented as

$$P(z_t = k \mid z_{t-1} = j) = A_{j,k}$$

Here z_t and z_{t-1} refer to the latent states at trials (t-1) and t, respectively. These latent states are hidden from the observers, and the state at each trial relies solely on the state of the preceding trial. The HMM also has an initial-state probability distribution over the first trial whose components sum to 1. The Bernoulli GLMs for each state specify how input variables govern decisions made by the animal by assigning a weight to each input variable. The animal's decisions are represented as 0 (left) and 1 (right). The input parameters for each option consist of signed stimulus contrast (z-scored across all trials), an internal bias term (uniformly set to 1), the animal's choice on the preceding trial ([-1,1]), and whether the previous trial was rewarded ([-1,1]).

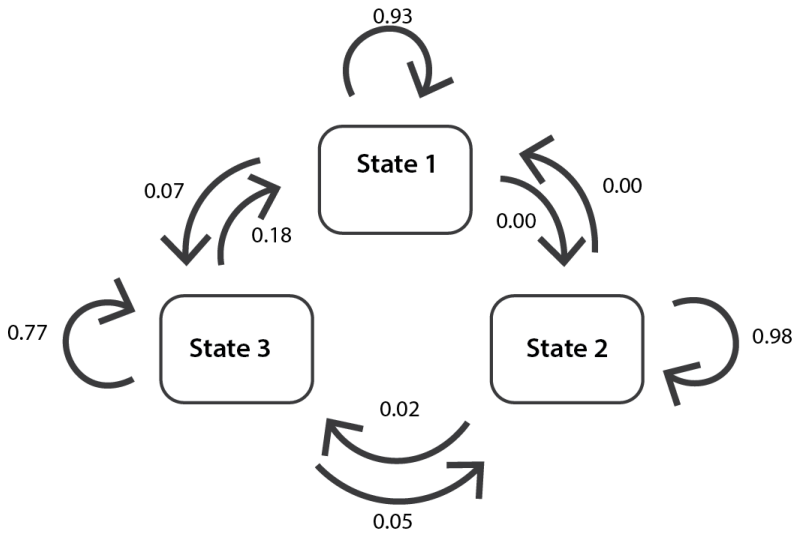

Figure 2.3: A schematic of 3-state GLM-HMM. The arrows represent the probabilities of transitioning into the next state. The probability values are inferred from the inferred global 3-state GLM-HMM. (Ashwood et al., 2022)

All parameters for the GLM-HMM, including the transition matrix, initial state distribution, state-specific GLMs, are learned from the animal's responses using the expectation-maximization (EM) approach. This approach tries to maximise the log-posterior of the parameters based on the choice and the input data with the forward-backward algorithm. To ensure unique initialisations when fitting the K-state global GLM-HMM, a gaussian noise with $= 0.2$ is introduced for each iteration. The global model yielding the highest training set log-likelihood is selected. To implement the GLM-HMM, version 0.0.1 of the Bayesian State Space Modeling framework developed

by Scott Linderman (https://github.com/lindermanlab/ssm) and its adaptation from Ashwood et al., 2022 (https://github.com/zashwood/glm-hmm) is used. Data from sessions after the mouse unlocked the final phase of the training paradigm are used for the GLM-HMM. Each mouse's data covers approximately 2500 to 3000 trials.

Multi-stage GLM-HMM fitting procedure (borrowed from Ashwood et al., 2022):

1. Fit GLM (one-state GLM-HMM) to the combined data of all animals.
2. Fit global GLM-HMM to the combined data of all animals:
   (a) Initialize K-state GLM-HMM using noisy GLM weights
   (b) Run the EM algorithm until convergence
3. Fit individual GLM-HMM to each animal:
   (a) Initialize K-state GLM-HMM using the global GLM-HMM parameters for this K
   (b) Run the EM algorithm until convergence

Refer to Ashwood et al., 2022, for more details on the execution of the GLM-HMM.

2.4.2 Cross-validation

We included 80% of the trials in the training set for each model fitting and 20% of the trials in the test set. The test sets were used to cross-validate each model. The log-likelihood of each model on the test set is reported in units of bits per trial (Ashwood et al., 2022) to make comparisons between models. It is represented as

$$\mathrm{LL}_{\text{bits per trial}} = \frac{\mathrm{LL}_{\text{test set}} - \mathrm{LL}_0}{n_{\text{test}} \log(2)}$$

Here, $\mathrm{LL}_{\text{test}}$ denotes the log-likelihood of the test set for a given model, and LL_0 signifies the log-likelihood of the same test set under a Bernoulli choice model. This null model assumes that the response side is decided by flipping a coin such that the probability of choosing a side is estimated as the fraction of trials the animal chooses that particular side. n_{test} refers to the total number of test set trials. An increase in log-likelihood value of 0.01 bits per trial for $\mathrm{n}_{\text{test}} = 1000$, refers to a 1024-fold higher probability of the test set being produced by the specified GLM-HMM.

2.5 Fibre photometry

2.5.1 Data acquisition

Neuronal activity from the LC is recorded using a Doric Lenses fibre photometry acquisition system consisting of a fibre photometry console, an LED driver, a fluorescence Mini Cube and a 200 μm thick 5 m long fibre-optic patch cord. TTL pulses from the behavioural acquisition system are recorded simultaneously to ensure syncing. GCaMP8f expressing cells in the LC are optically stimulated at 470 nm wavelength for calcium-dependent excitation and 405 nm wavelength for isosbestic excitation. Both signals are separated in real time using distinct input frequencies through lock-in demodulation of the LED driver. The current output is adjusted to ensure 0.04 mW excitation power at the tip of the fibre. All inputs are recorded at a 12 kHz sampling rate. Before each recording day, light with maximum power (at 470nm and 405nm) is passed through the patch cord for a minimum of 20 minutes to photobleach autofluorescence within the patch cord and improve recording quality.

2.5.2 Signal processing

All fibre photometry signals recorded are preprocessed and normalised using custom Python scripts with available packages like NumPy, Matplotlib, pandas, and SciPy. Calcium-dependent and isosbestic wavelength signals for each session are low-pass filtered at 5 Hz to remove high-frequency noise. Each signal is individually fitted with a polynomial of five degrees to estimate changes in the baseline due to photobleaching. The signals are individually divided by their baseline to correct for slow decreases in fluorescence over time. The corrected calcium-dependent signal is subtracted by the corrected isosbestic signal to correct for signal artefacts generated by movement. This normalised dF/F signal is further z-scored per trial or session, as indicated later with each analysis to remove variations across mice, sessions and trials.

2.5.3 Event-specific analysis

Event-specific traces are extracted from 2 s before to 2 s after the event. Each trace is z-scored using trace-specific baselines.

$$z\text{-score} = \frac{x - \mu_{\text{baseline}}}{\sigma_{\text{baseline}}}$$

Here, x is the trace value at a given time, μ_{baseline} is the baseline average, and σ_{baseline} is the baseline standard deviation. This baseline signal is defined as

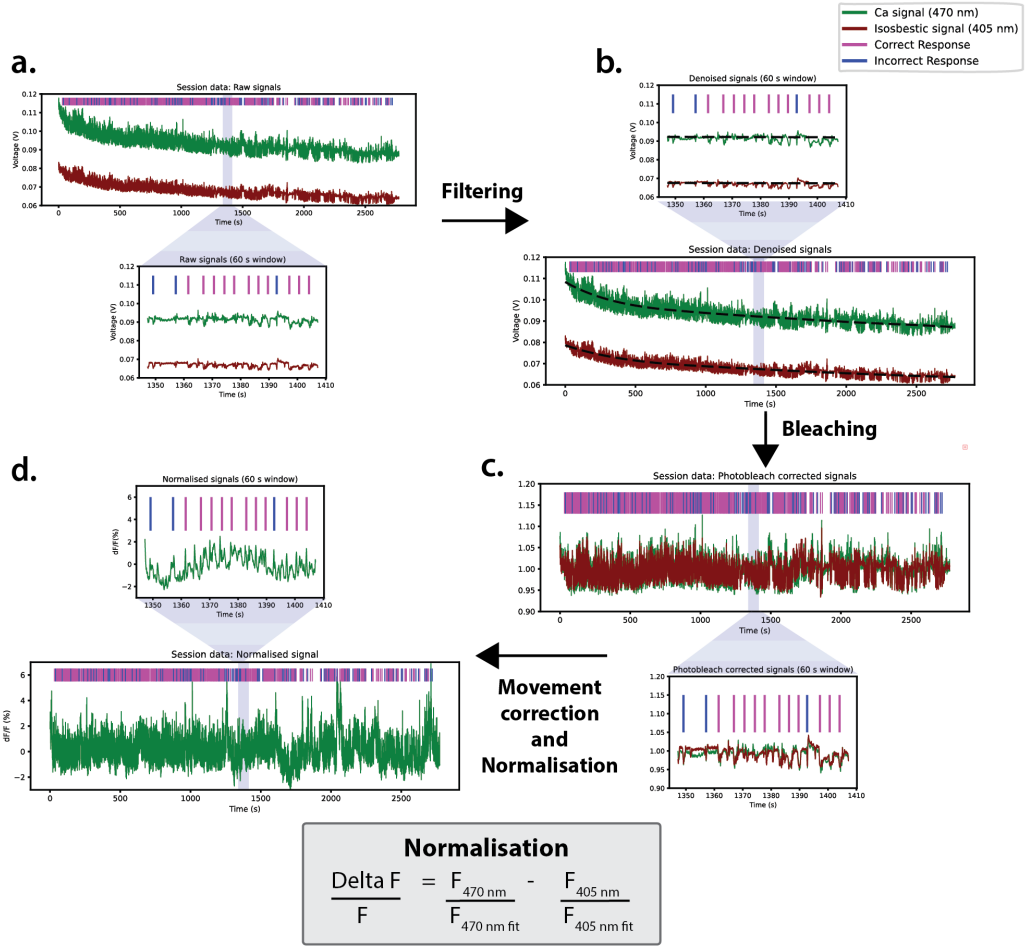

Figure 2.4: Fibre photometry signal processing pipeline: **a.** Raw fibre photometry signals for calcium activity in maroon (470 nm wavelength) and isosbestic signal in green (405 nm); **b.** Denoised signals with their respective polynomial curve fit (in black dashed-line); **c.** Bleaching corrected signals, **d.** Movement corrected and normalised signal. Each preprocessing step is represented by signals for the whole session and a 60 s window. Correct and Incorrect response TTLs are represented in magenta and blue, respectively.

the average signal within the time window from 2 s before to 1 s before the event. The event-specific peaks are identified using the find_peaks function of the scipy.signal package. The peak prominence cut-off is set at 0.5 to ensure that only significant local minima are detected. To identify troughs, the signal is multiplied by -1 and negative peaks are identified using the same approach.

For calculating event-specific baseline calcium activity, each session signal is z-scored. This removes signal variations between sessions and mice while maintaining baseline activity variations between trials.

$$z\text{-score} = \frac{x - \mu_{\text{session}}}{\sigma_{\text{session}}}$$

Here, x is the signal value at a given time, μ_{baseline} is the session average, and σ_{baseline} is the session standard deviation. The baseline activity for a period of interest is calculated by averaging the signal in that time window.

Chapter 3

Results

3.1 Learning in mice during perceptual decision-making task

We started with training DBH-cre transgenic mice in the behavioural paradigm. These mice were injected with cre-dependent GCaMP8f expressing viral vectors in the LC. In this behavioural task, the mice are presented with a visual stimulus on a screen's right or left side. They have to learn to turn a wheel in a direction to bring the stimulus to the centre. If the visual stimulus is presented on the right in a trial, the mouse must learn to move the wheel to the left and vice versa. Each correct response is rewarded with a drop of 10% sucrose water, while a noise burst follows incorrect responses and timeouts. To increase task difficulty, the contrast of the visual stimulus varies from 100% to 0% in each trial. The training paradigm begins with 100% and 50% contrasts. Successively, lower contrasts are added or removed in each stage as the mouse learns to perform accurately in the previous stage (explained in detail in the Methods section). We found that all injected DBH-cre mice (n=4) bred in our animal facility failed to learn this task within 45 training days. To probe this further and test if this resulted from the mouse line, viral injections in the LC or our execution of the behavioural paradigm, we switched to other available mouse lines while maintaining the protocol for LC injections. We trained B6J control (n=3), TH-cre (n=6), DBH-cre X hTyr X Ai9 (n=1), DBH-cre X hTyr (n=1) mice. Out of these mice (n=11), most (n=7) learned the behavioural paradigm within 45 days, while one mouse suffered a stroke within a week of starting the training paradigm. LC is located deep in the brainstem, which is why the survival rate of mice after stereotactic injections is low. Out of 24 injected mice, only 18 mice survived long enough to start training without observable neurological deficits [Fig.

3.1a]. We also injected B6J mice (n=4) with non-cre-dependent GCaMP8f expressing virus. Out of these, three mice survived and learned the training paradigm. The mean accuracy across training sessions for mice from each genetic background is presented in Fig. 3.1b. We successfully trained 10 mice in this behavioural paradigm [Fig. 3.1c].

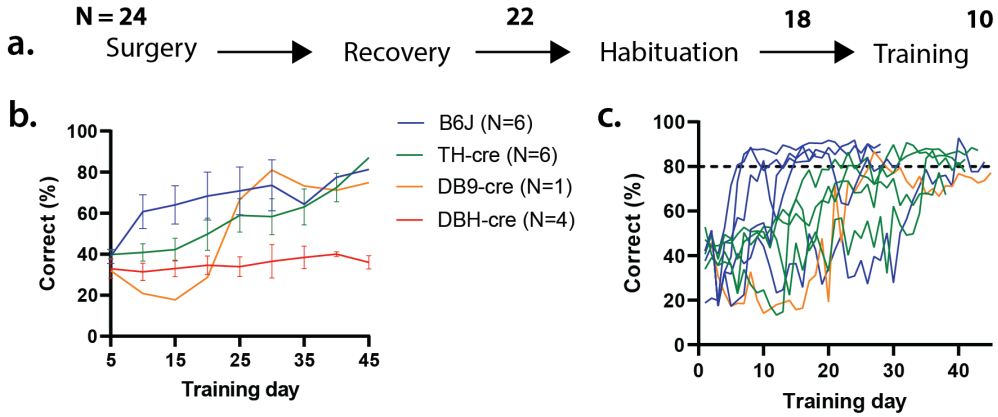

Figure 3.1: Learning trajectory during the perceptual decision-making task in mice. **a.** Experimental paradigm with the total number of mice at each stage.; **b.** Mean accuracy across training sessions for each mouse line (error bars: SEM). Each colour represents a distinct mouse line; **c.** Accuracy across training sessions for individual mice that learned (n=10).

Mice show variations in individual learning rates [Fig. 3.1c], which may result from the following reasons. The behavioural paradigm requires the mice to be comfortable moving the wheel in both directions with their forepaws. At the beginning of the training paradigm, some mice are observed to use a single dominant forepaw (right/left) while others move the wheel with both paws. This differential forepaw dominance in mice varies the ease with which the mice move the wheel and respond appropriately to the task. Another reason for differential learning rates may be individual differences in motivation levels.

Fig.3.2 shows the distribution of response times of mice after learning the task. This is calculated as the duration from the start of a trial till a choice is registered. These ranged from 0.60 s to 65.42 s.

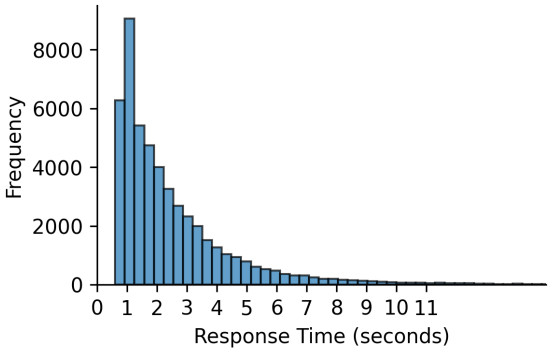

Figure 3.2: Response time distribution after learning (n = 10 mice).

3.2 Global LC neuronal dynamics during the behavioural task.

We recorded calcium activity in the LC-NA neurons during the behavioural task using fibre photometry. Optical fibres were implanted in the LC region unilaterally, and recordings were taken during each training session. LC-NA neurons are known to respond phasically to salient stimuli. This phasic activity is observed before a choice is made during conditioning tasks and is linked to modulating decision-making processes and cognitive / attentional shifts (Aston-Jones and Cohen, 2005; Bouret and Sara, 2005). We used data from trained transgenic mice, TH-Cre (n=3) and DBH-Cre x hTyr x Ai9 (n=1), expressing GCaMP8f in the locus coeruleus. We looked at task event-specific average calcium activity in the locus coeruleus. Each event-specific signal trace was z-scored using pre-event baselines. We analysed the averaged trace for correct and incorrect trials for all mice together [Fig. 3.3a]. We found that the average calcium activity across the trials peaks just before a choice response is registered. This peak in calcium levels drops after the choice is made. This drop is faster for the correct trials. We also averaged the calcium traces for choice events when the mouse chooses the right vs the left side [Fig 3.3d].

We followed this with summary statistics. We analysed the average amplitude of the highest peak within 500 ms before a choice was made. This amplitude is significantly higher for correct trials compared to incorrect trials [Fig. 3.3b]. Unlike in go/no-go operant conditioning and signal detection behavioural paradigms, all stimuli presented here are salient and associated with reward. We also looked at maximum peak amplitudes just before a choice is made (within 500 ms) when the animal chooses the left vs right

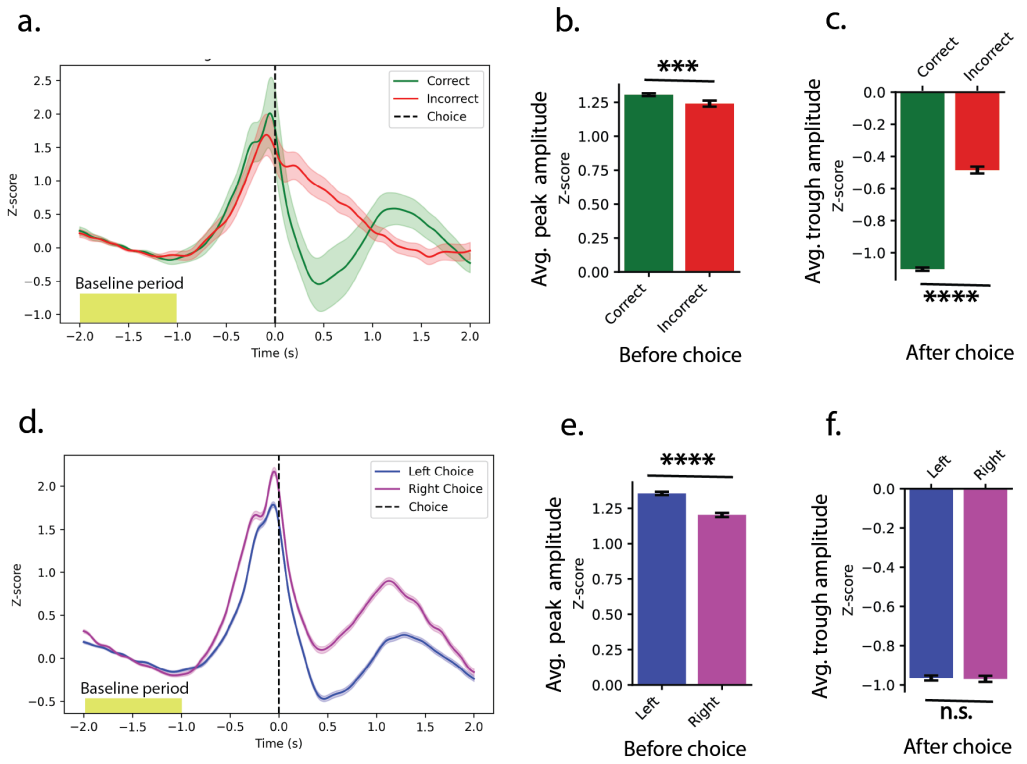

Figure 3.3: LC neuronal dynamics after learning at choice time for population data (4 mice). **a.,d.** Average trace with SEM for all trials referenced to choice time. Each trace is z-scored using the signal from the baseline period; **b.** Average peak amplitude within 500 ms before a choice is registered for all trials (error bars: SEM), Man-Whitney U statistic = 7402299, p-value<0.001, $n_{correct}$ = 7527 trials, $n_{incorrect}$ = 1865 trials; **c.** Average trough amplitude within 500 ms after a choice is registered for all trials (error bars: SEM), Man-Whitney U statistic = 2890642, p-value<0.0001, $n_{correct}$ = 5930 trials, $n_{incorrect}$ = 1667 trials; **e.** Average peak amplitude within 500 ms before a choice is registered for all trials (error bars: SEM), Man-Whitney U statistic = 11716571, p-value<0.0001, n_{left} = 5552 trials, n_{right} = 3840 trials; **f.** Average trough amplitude within 500 ms after a choice is registered for all trials (error bars: SEM), Man-Whitney U statistic = 7027083, p-value is not significant, n_{left} = 4541 trials, n_{right} = 3056 trials. Table A.2 in the Appendix describes the distribution of trials included from each mouse.

side. The average peak amplitudes for left choices were significantly greater than that for the right choices [Fig. 3.3e]. We also found that the average minimum trough amplitude within 500 ms after the choice was made was significantly lower for the correct trials than the incorrect trials [Fig. 3.3c]. No differences were seen in average trough amplitudes after right and left choices [Fig. 3.3f]. The difference in this average trough amplitude with respect to the wheel response side was not significant.

During the engagement with task-relevant stimuli, LC-NA neurons show low / moderate tonic activity with phasic responses. Very low or high tonic activity is associated with disengagement from task-relevant stimuli and exploration of alternate strategies in the environment. We averaged calcium activity traces during the trial start for all mice [Fig. 3.4a, c]. We looked at the baseline activity of LC-NA neurons within 500 ms of stimulus presentation. The overall average signal across all trials for all mice was 0.76 z-score. The average baseline after the start was -0.01 z-score. This average baseline just after a trial starts/ stimulus presentation is 113% less than the overall average LC-NA activity. The average baseline signal after stimulus presentation for correct trials was significantly lower than for incorrect trials after learning [Fig. 3.4b]. This observation was not observed before learning in mice that learned the task [Fig. 3.5a]. It was also not observed in mice that did not learn the task (n = 5 mice: 3 DBH-cre, 2 TH-cre) [Fig. 3.5c]. No significant differences were found in this average baseline with respect to the response side chosen in each trial [Fig. 3.4d].

Figure 3.6 shows the average LC calcium traces for individual mice referenced to choice time after learning. TH-cre Mo2 and Mo3 have high threshold parameters for the psychometric curves (Table 3.1). These mice also show more prominent peaks in average calcium traces at choice time for correct trials compared to incorrect trials. The average LC calcium trace corresponding to the inferred bias side of the psychometric curves (negative bias: left bias, positive bias: right bias) is observed to have a lower trough just after a choice is registered. The response side with a higher average peak before choice may correspond to the bias to the response side during initial learning sessions for the respective mice. Refer to Figure A.1b in the Appendix for initial response side bias during learning.

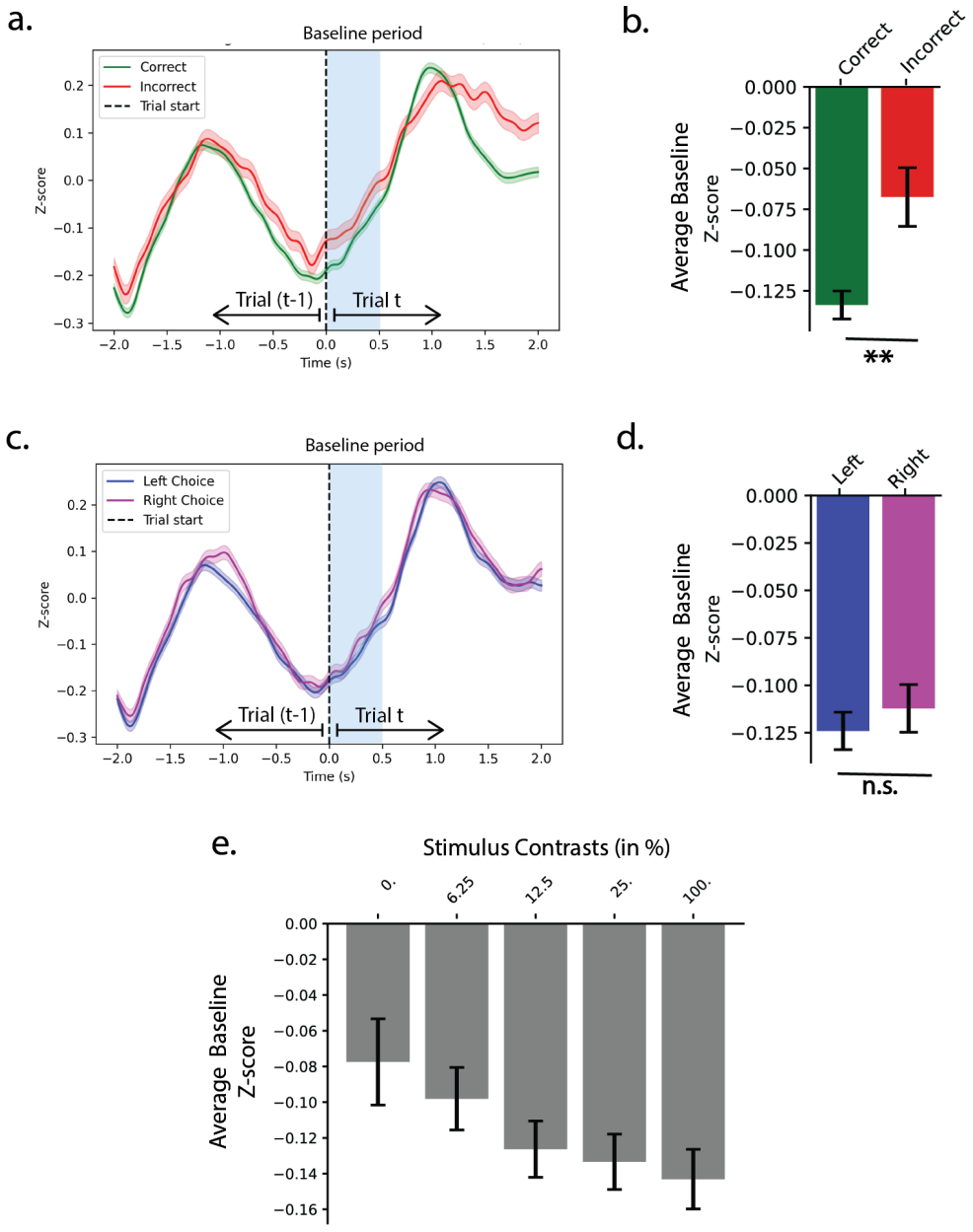

Figure 3.4: LC neuronal dynamics after learning at trial start for population data (4 mice). **a.,c.** Average calcium trace with SEM for all trials referenced to trial start time; **b.** Average baseline for all trials within 500 ms after a trial starts (error bars: SEM), Man-Whitney U statistic = 9535823, p-value < 0.01, $n_{correct}$ = 8468 trials, $n_{incorrect}$ = 2346 trials; **d.** Average baseline for all trials within 500 ms after a trial starts (error bars: SEM), Man-Whitney U statistic = 13990898, p-value = not significant, n_{left} = 6500 trials, n_{right} = 4314 trials. Table A.2 in the Appendix describes the distribution of trials included from each mouse.

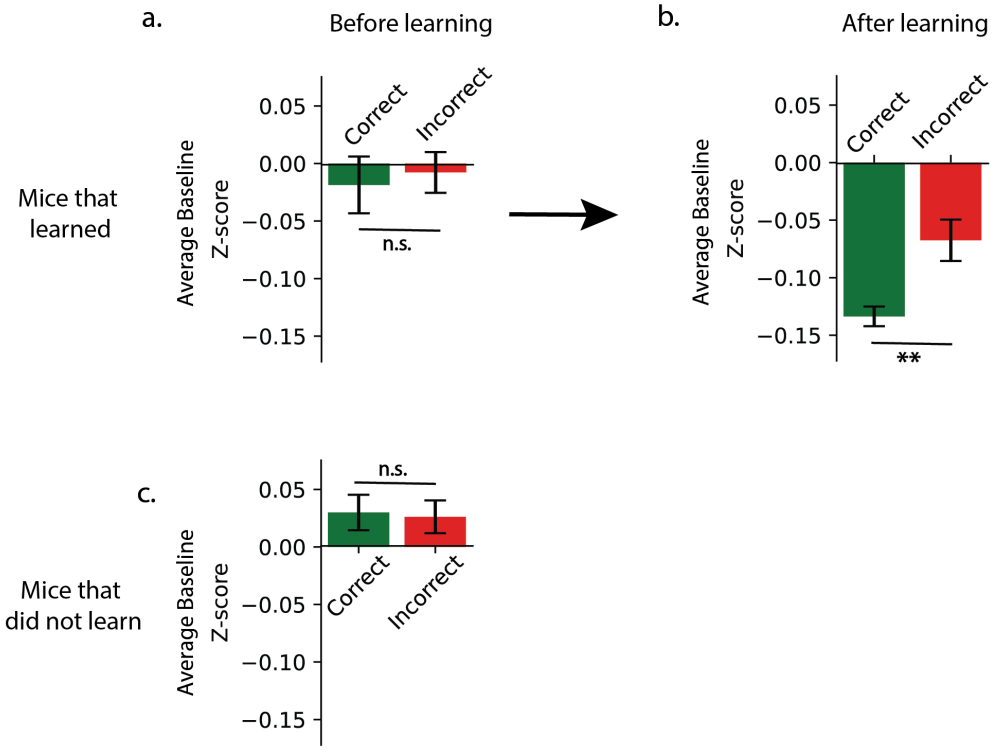

Figure 3.5: LC neuronal dynamics with respect to learning at trial start for population data. **a.** Average baseline within 500 ms after a trial starts before learning for mice that learned the task (n = 4 mice, error bars: SEM), Man-Whitney U statistic = 2079153, p-value = not significant, $n_{correct}$ = 1506 trials, $n_{incorrect}$ = 2815 trials; **b.** Average baseline within 500 ms after a trial starts after learning for mice that learned the task (n = 4 mice, error bars: SEM), Man-Whitney U statistic = 9535823, p-value < 0.01, $n_{correct}$ = 8468 trials, $n_{incorrect}$ = 2346 trials; **c.** Average baseline within 500 ms after a trial starts for mice that did not learn the task (n = 5 mice, error bars: SEM), Man-Whitney U statistic = 3805695, p-value = not significant, $n_{correct}$ = 2384 trials, $n_{incorrect}$ = 3146 trials.

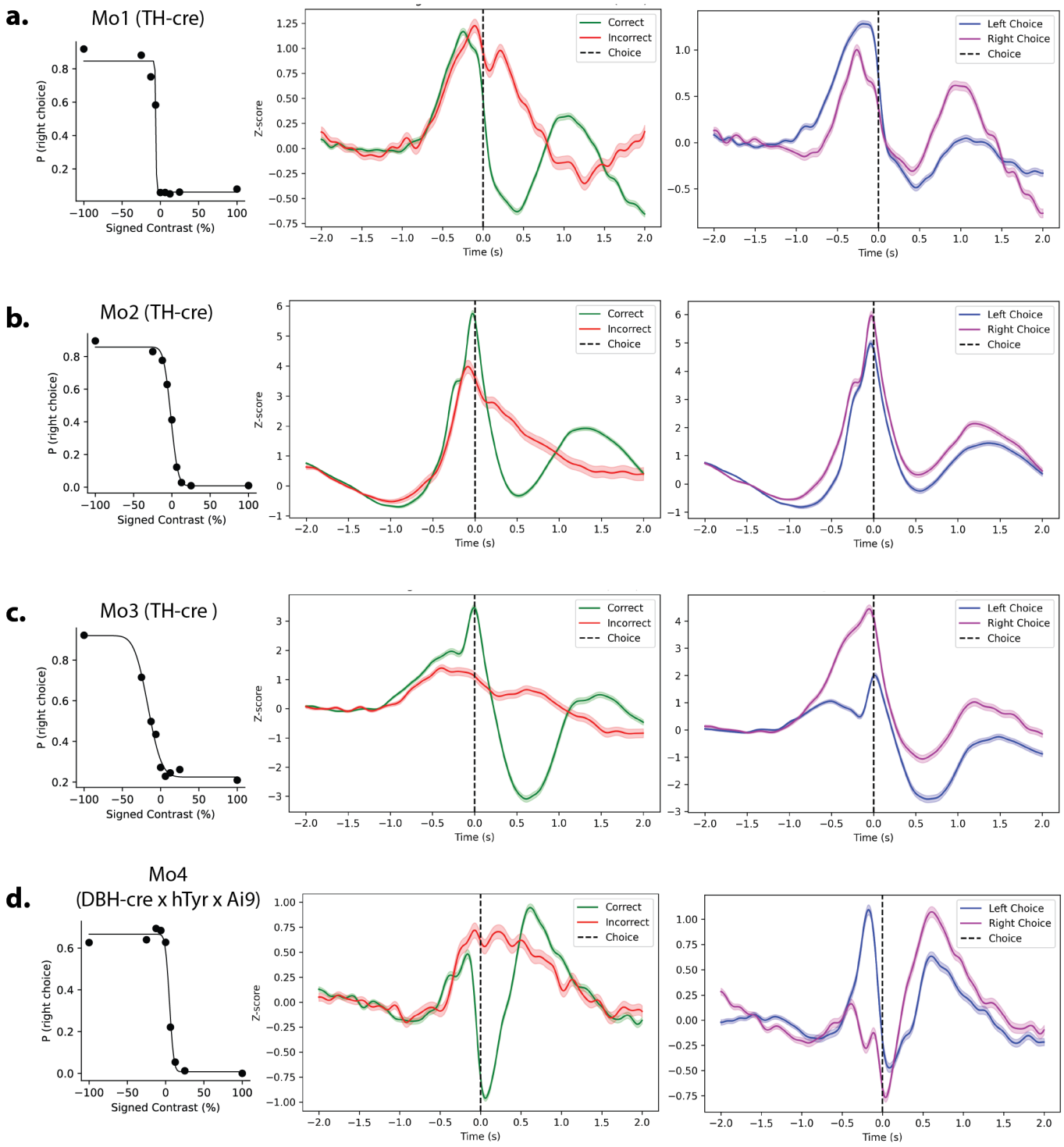

Figure 3.6: Choice-event specific LC dynamics and task behaviour for individual mouse. (From left) Task behaviour psychometric curve, Average calcium trace referenced to choice time for all correct and incorrect trials, Average calcium trace referenced to choice time for all trials with left and right choices for each mouse.Table A.2 in the Appendix describes the distribution of trials included from each mouse.

Mouse	Bias	Threshold	High lapse rate	Low lapse rate
Mo1 (TH-cre)	-5.92	1.11	0.15	0.06
Mo2 (TH-cre)	-1.39	10.51	0.14	0.01
Mo3 (TH-cre)	-16.57	19.94	0.08	0.22
Mo4 (DBH-cre x hTyr x Ai9)	5.07	6.15	0.33	0.01

Table 3.1: Inferred psychometric curve parameters for individual mice after learning

3.3 Fitting GLM-HMM to identify attentional states

To identify attentional states displayed by mice during this behavioural task, we modelled attentional states as hidden states in a hidden Markov model [Ashwood et al., 2022]. We fit a GLM (1-state) and K-state GLM-HMM (K=2,3,4,5) with data from 10 trained mice after they had successfully learned the task (reached the final stage of the training paradigm). Our dataset included $>$ 2500 trials for each mouse across multiple sessions. We fit a set of models with global data comprising pooled data from all 10 mice and another set of models for each individual animal. The models were fit with four inputs: signed stimulus contrast, constant bias term, the choice made in the previous trial, and whether or not the animal was rewarded in the previous trial.

Like Ashwood et al. (2022), we found that multi-state GLM-HMM outperformed the simple GLM in the testset log-likelihood [Fig.3.7a]. Although the improvement in test log-likelihood in Ashwood et al., 2022 only started leveling off after 3 states, we observed this levelling off after 2 states. We propose that for our fitted model, the 2-state GLM-HMM is sufficient to describe decision-making strategies employed during this task. Refer to Appendix Figure A.2 for inferred model parameters from Ashwood et al., 2022. For reproducibility, we decided to delve into the 3-state GLM-HMM describing 3 attentional states. The inferred transition matrix for the 3-state model shows the probabilities of transitioning to states [Fig. 3.7b]. The diagonal elements have high probabilities, showing that mice tend to stay in the same state for multiple trials. The inferred GLM weights quantify the dependency of choice made by mice on the respective input parameters [Fig. 3.7c]. In this

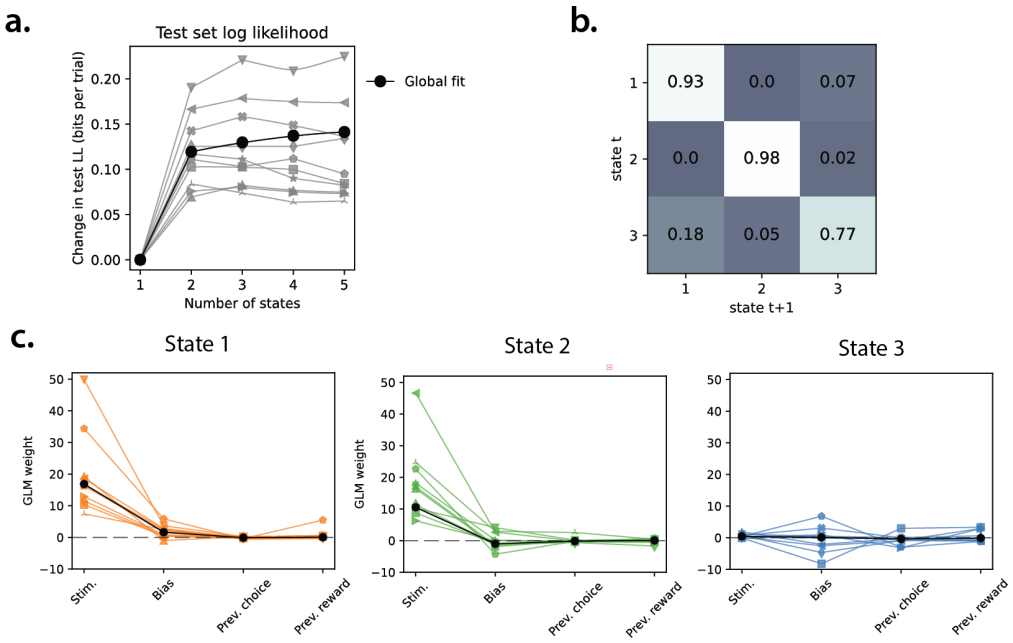

Figure 3.7: Fitting GLM-HMM model (Ashwood et al., 2022) to data from trained mice (n=10 mice). **a.** Change in test log-likelihood as a function of the number of states relative to (one-state) GLM. Each grey trace represents fit for an individual mouse. Black trace represents global fit using pooled data from all selected mice; **b.** Inferred transition matrix for three-state GLM-HMM for global fit; **c.** Inferred GLM weights for each of the three states in the three-state GLM-HMM. Each coloured trace represents fit for an individual mouse. Black trace represents the global fit.

behavioural task, the optimal strategy is to have high weights for the stimulus, while negligible weights for the other three parameters. Two inferred states showed high dependency on the stimulus and low dependency on other parameters. These two 'engaged' states differ slightly in the degree of dependence on the internal bias term. The third state has low dependency on the stimulus and can be referred to as a 'disengaged state'. The state GLMs for individual mice are initialised with the global GLM weights during fitting. This ensures that each inferred latent state can be mapped across individuals and the global fit giving us similar states between individuals and the global fit.

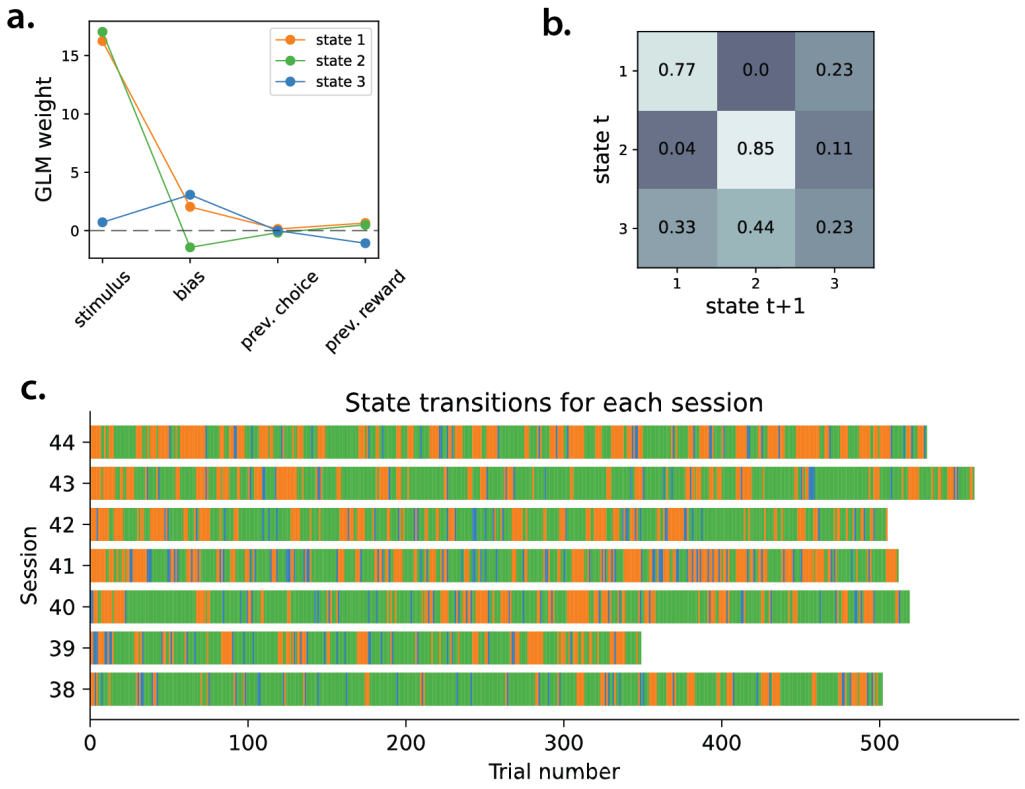

Figure 3.8: 3-state GLM-HMM model (Ashwood et al., 2022) fitting to data from an example mouse (n 3000 trials). **a.** Recovered GLM weights; **b.** Recovered HMM transition matrix; **c.** Predicted state transitions for each session through posterior probabilities. Each state is represented by a distinct colour.

To predict the attentional states employed by a mouse during trials in a session, we calculated posterior probabilities using the inferred 3-state GLM-

HMM. Fig. 3.8c shows the state transitions across trials for an example mouse. The mice tend to switch states multiple times within a single session. These transitions are predicted by our model, given the observed inputs and choices in a session. The example mouse prefers to stay in the engaged states. It spends around 61% of the trials in state 2, 30% in state 1 and 8% in state 3.

3.4 LC neuronal dynamics during attentional states.

We looked at the LC-NA neuronal calcium activity during these attentional states (n = 4: 3 TH-Cre and 1 DBH-Cre x hTyr x Ai9 mouse) [Fig. 3.9a]. We used the global fit to predict attentional states during trials for these four mice using posterior probabilities. We fit a psychometric curve to the pooled behavioural data for each state [Fig. 3.9b] to understand the behavioural strategies in each state. State 1 and state 2 have similar threshold parameters, representing similar stimulus contrast sensitivity. These 'engaged' states differ in the bias parameter of the psychometric curve with state 1 and 2 biased towards the left and right side respectively. State 3 is associated with high lapse rates denoting low accuracy for high stimulus contrast trials. This state can be referred to as the 'disengaged state'. These states have task accuracy of 88%, 93% and 28%, respectively [Figure 3.9c].

Low average baseline calcium activity is observed in the LC just after start (within 500 ms) for trials. This baseline activity is significantly lower for trials in the 'engaged' states than those in the 'disengaged state' [Figure 3.9d]. These inferred states are associated with the low threshold parameter for the inferred psychometric curve signifying high sensory sensitivity for stimulus contrasts in expert mice.

Average LC calcium peak amplitude for trials in state 1 just before a choice is registered is significantly higher than that for trials in state 2 and state 3 [Figure 3.9e]. The magnitude of bias in the inferred psychometric curve parameters is also larger for state 1 than for state 2 and 3.

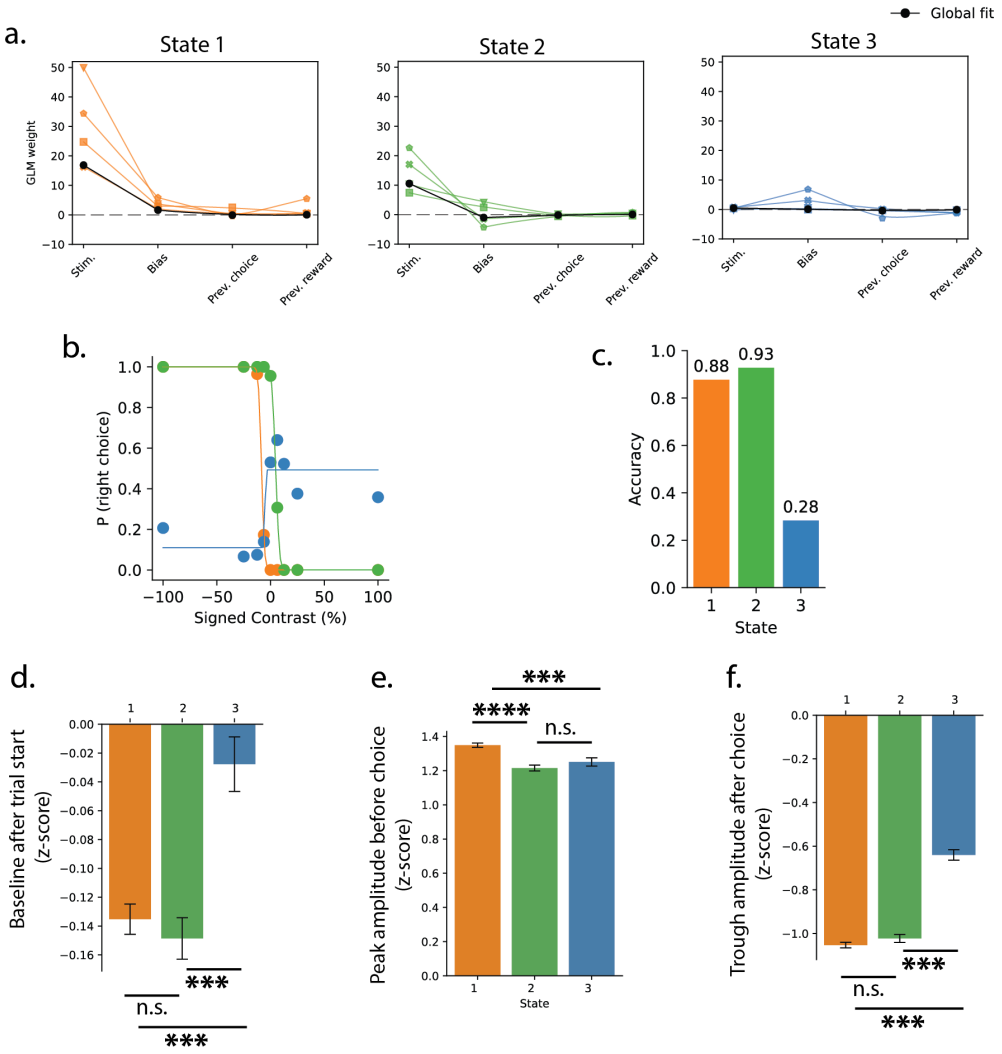

Figure 3.9: LC neuronal dynamics during attentional states after learning for population data (n = 4 mice with GCaMP expression in the LC). **a.** Recovered GLM weights for 3-state GLM-HMM. Black trace represents global fit. Coloured trace represents individual mouse fit; **b.** Inferred psychometric curve for each state. The states during trials are predicted through posterior probabilities; **c.** Accuracy during trials in each attentional state; **d.** Average baseline for all trials within 500 ms after a trial starts (error bars: SEM). One-way ANOVA with Bonferroni correction: ANOVA F-statistic = 15.90535866, p-value < 0.0001, $n_{state\ 1} = 5742$ trials, $n_{state\ 2} = 3097$ trials, $n_{state\ 3} = 1977$ trials **e.** Average peak amplitude for all trials within 500 ms before a choice is registered (error bars: SEM). One-way ANOVA with Bonferroni correction: ANOVA F-statistic = 15.90535866, p-value $<$ 0.0001, $n_{state\ 1} = 5013$ trials, $n_{state\ 2} = 2770$ trials, $n_{state\ 3} = 1610$ trials**f.** Average trough amplitude for all trials within 500 ms after a choice is registered (error bars: SEM). One-way ANOVA with Bonferroni correction: ANOVA F-statistic = 15.90535866, p-value < 0.0001, $n_{state\ 1} = 4021$ trials, $n_{state\ 2} = 2136$ trials, $n_{state\ 3} = 1441$ trials. All Bonferroni pairwise comparison p-values are represented on the respective graphs. A distinct colour represents each state. Table A.2 in the Appendix describes the distribution of trials included from each mouse.

State	Bias	Threshold	High lapse rate	Low lapse rate
1	-8.39	3.17	0.00	0.00
2	4.75	3.88	0.00	0.00
3	-5.25	0.99	0.89	0.49

Table 3.2: Inferred psychometric curve parameters for predicted states in 3-state GLM-HMM

Chapter 4

Discussion

We identified three attentional states shown by mice when making decisions during a perceptual decision-making task using a 3-state GLM-HMM. These attentional states include two 'engaged' states where mice's responses show high task stimulus dependency. The mice can respond to this behavioural task by moving a wheel in two directions. The 'engaged' states differ in the bias shown by mice to a specific response direction. The third attentional state is a 'disengaged' state with low task stimulus-dependence. This 'disengaged' state, persisting for 18% of the total trials, is associated with high lapse rates. We explored the calcium activity dynamics of the noradrenergic LC neurons during these attentional states through fibre photometry recordings. Calcium activity in the LC shows significant differences between these states. We discuss the important findings of this study below.

4.1 Cognitive impairment in DBH-Cre mouse line

Inbred mouse models are a very valuable tool for biological research. They provide genetically and phenotypically consistent traits promoting reproducibility across experiments and laboratories. Genetic modifications can be introduced in established inbred mouse lines to generate transgenic mouse models. We discovered differential learning rates in the perceptual decision-making task between the DBH-cre mouse line bred in our animal facility and mice from another genetic background. Mice from the DBH-cre mouse line failed to learn this highly standardised behavioural task. This mouse line is widely used across other labs to study locus coeruleus.

One hypothesis can be that our lab's DBH-cre mouse colony has undergone a genetic drift affecting cognitive learning abilities during behavioural

tasks. Transgenic mouse lines are susceptible to spontaneous neutral genetic mutations that may spread and become fixed in a mouse colony over generations. These mutations induce phenotypic differences that significantly influence research and reproducibility. Genetic drift is more prominent in smaller colonies of mice. The effects of genetic drifts can be mediated by back-crossing to the inbred control line every 5-10 generations to refresh the genetic background. When we trained a DBH-cre x hTyr mouse crossed with an Ai9 mouse line, the mouse could successfully learn the task. Before future behavioural experiments with the same mouse line, we propose back-crossing the transgenic mouse colony in our animal facility with their inbred control background (C57BL/6).

Another possible reason for this cognitive impairment may be neurological impairments caused by optical fibre placements over the vulnerable nucleus, LC. We trained three C57BL/6J mice as a control with the same injection and optical fibre implant coordinates. These mice successfully learned the task. We also tried a range of injection sites with other genetic mouse lines to test its effect on cognitive impairment [Table 2.1]. We found no significant changes in learning rates between mice with different injection sites.

Our dataset is small, and we cannot account for the exact reason for this impairment. We want to highlight the effects of the genetic background of mice in behavioural experiments and good breeding practices, including accounting for genetic drift while maintaining mouse colonies.

4.2 LC neuronal dynamics during attentional states

Fibre photometry records population-level calcium activity from neurons. We used GCaMP8f, which was injected into the LC, to examine calcium activity during this task. GCaMP8f has very fast dynamics. It has a half-decay time of less than 100 ms when expressed in the visual cortex and cerebellar Purkinje neurons, recorded with 2-photon microscopy (Zhang et al., 2023). We look at tonic and phasic activity in the locus coeruleus. Distinguishing calcium dynamics associated with distinct firing patterns is tricky while looking at population-level recordings such as fibre photometry. We classify averaged signal during the time of interest as baseline tonic activity and signal peaks as task event-specific phasic calcium activity. A low tonic firing rate produces a lower calcium signal in fibre photometry.

We found significant differences between LC calcium activity parameters for the three states. We choose the trial start and choice time as our time

of interest. We found an overall 113% less average LC baseline calcium activity just after the stimulus is presented (within 500 ms) compared to the overall average calcium signal across all trials for all mice. This tonic baseline activity just after stimulus presentation/trial start for engaged states showed a significantly lower average for trials predicted to be in the 'engaged' states. We also found this to be significantly lower for stimulus presented for all trials with correct responses than incorrect ones. As each stimulus is salient in this behavioural task, all stimuli presentations are associated with low LC baseline activity. The degree of this reduction can be linked to the task accuracy and stimulus sensitivity in each state.

This observation aligns with the adaptive gain theory that proposes engagement during task-relevant stimuli is associated with phasic LC responses and moderate LC tonic firing (Aston-Jones & Cohen, 2005). Meanwhile, very high tonic activity periods are associated with disengagement from the task. It also aligns with the network reset theory, which proposes reduced LC activity during active attention to prevent cognitive shifts (Bouret & Sarah, 2005). Dahl et al., 2022 also showed that moderate NA activity during an auditory signal detection task was associated with optimal performance. Another recent paper showed that moderate tonic LC activation engages associative processing regions, and phasic stimulation biases the brain to sensory processing (Grimm et al., 2024). Our results contradict the study by Bari et al., 2020 which showed consistently higher spontaneous LC activity during the delay period before correct responses compared to wrong/omitted responses in a two-choice task.

Our data for fibre photometry analysis is derived from 4 mice with 3 TH-cre mice (2 males and one female) and 1 DBH-cre x hTyr x Ai9 male mouse. The number of mice included in our study is low, with variations in genetic backgrounds. However, we have included calcium activity data from over 10,000 trials after the mice learnt this task. Two mice from this cohort had a $\leq 1\%$ Δ F/F range for some sessions. These sessions were also included in the dataset, and the data was pooled after z-scoring. Our LC recording shows a low signal-to-noise ratio due to the following reasons. LC is a small nucleus from which a subset of neurons get transfected with GCaMP. The optical fibre implant also samples only a subpopulation of neurons close to the implant. LC neurons are tonically active. This results in an elevated calcium signal as noise, making it challenging to distinguish relevant signal variations.

Our results show that locus coeruleus neurons show differential activity during predicted attentional states in a perceptual decision-making task in mice. Lower average baseline activity just after stimuli presentation (within 500 ms) seems to be linked to higher task accuracy and stimulus sensitivity

in each attentional state. We propose that average baseline activity may be used to predict engagement and accuracy in this task. Future work will study pupil dynamics during these attentional states and their correlation with LC neuronal dynamics. We have recorded pupil size changes during the training sessions through infrared cameras, which can be extracted through DeepLabCut (Mathis et al., 2018). Here, in this work, we established the key role of the LC in accuracy and performance in a decision-making task in mice.

References

Arnsten AF, Goldman-Rakic PS (1984). Selective prefrontal cortical projections to the region of the locus coeruleus and raphe nuclei in the rhesus monkey. Brain res 306:9–18.

Arnsten AF, Wang MJ, Paspalas CD (2012). Neuromodulation of thought: flexibilities and vulnerabilities in prefrontal cortical network synapses. Neuron 76:223–239.

Ashwood, Z.C., Roy, N.A., Stone, I.R. et al. Mice alternate between discrete strategies during perceptual decision-making. Nat Neurosci 25, 201–212 (2022).

Aston-Jones G, Cohen JD. Adaptive gain and the role of the locus coeruleus-norepinephrine system in optimal performance. J Comp Neurol. (2005).

Azevedo, F.A.C., Carvalho, L.R.B., Grinberg, L.T., Farfel, J.M., Ferretti, R.E.L., Leite, R.E.P., Filho, W.J., Lent, R. and Herculano-Houzel, S. Equal numbers of neuronal and nonneuronal cells make the human brain an isometrically scaled-up primate brain. J. Comp. Neurol. (2009)

Benarroch EE. Locus coeruleus. Cell Tissue Res. 2018 Jul;373(1):221–232.

Bouret S, Sara SJ. Network reset: a simplified overarching theory of locus coeruleus noradrenaline function. Trends Neurosci. 2005 Nov;28(11):574-82.

Dahl, M.J., Mather, M., Werkle-Bergner, M., 2022. Noradrenergic modulation of rhythmic neural activity shapes selective attention. Trends Cogn. Sci. 26 (1)

Downs JL, Dunn MR, Borok E, Shanabrough M, Horvath TL, Kohama SG, Urbanski HF (2007). Orexin neuronal changes in the locus coeruleus of the ageing rhesus macaque. Neurobiol Aging 28: 1286–1295

Ginsberg SD, Hof PR, Young WG, Morrison JH (1993). Noradrenergic innervation of the hypothalamus of rhesus monkeys: distribution of dopamine-beta-hydroxylase immunoreactive fibres and quantitative analysis of varicosities in the paraventricular nucleus. J Comp Neurol 327:597–611

Golmayo, L.; Nunez, A.; Zaborszky, L. Electrophysiological evidence for the existence of a posterior cortical-prefrontal-basal forebrain circuitry in modulating sensory responses in visual and somatosensory rat cortical areas. Neuroscience 2003, 119, 597–609.

Grimm, C., Duss, S.N., Privitera, M. et al. Tonic and burst-like locus coeruleus stimulation distinctly shift network activity across the cortical hierarchy. Nat Neurosci 27, 2167–2177 (2024).

Hagena H, Hansen N, Manahan-Vaughan D (2016). Beta-adrenergic control of hippocampal function: Subserving the choreography of synaptic information storage and memory. Cereb Cortex 26:1349–1.

Hansen, J.Y., Shafiei, G., Markello, R.D. et al. Mapping neurotransmitter systems to the structural and functional organization of the human neocortex. Nat Neurosci 25, 1569–1581 (2022).

Hickey, L., Li, Y., Fyson, S. J., Watson, T. C., Perrins, R., Hewinson, J., Teschemacher, A. G., Furue, H., Lumb, B. M., & Pickering, A. E. (2014). Optoactivation of locus coeruleus neurons evokes bidirectional changes in thermal nociception in rats. Journal of Neuroscience, 34(12), 4148–4160.

Jones BE, Moore RY. Ascending projections of the locus coeruleus in the rat. II. Autoradiographic study. Brain Res. 1977 May 20;127(1):25–53.

Jordan G McCall, Edward R Siuda, Dionnet L Bhatti, Lamley A Lawson, Zoe A McElligott, Garret D Stuber, Michael R Bruchas (2017). Locus coeruleus to basolateral amygdala noradrenergic projections promote anxiety-like behavior. eLife 6:e18247.

Jordan R, Keller GB. The locus coeruleus broadcasts prediction errors across the cortex to promote sensorimotor plasticity. Elife. 2023 Jun 7;12:RP85111.

Jordan R, Keller GB. The locus coeruleus broadcasts prediction errors across the cortex to promote sensorimotor plasticity. Elife. 2023 Jun 7;12:RP85111.

Jordan R. The locus coeruleus as a global model failure system. Trends Neurosci. 2024 Feb;47(2):92-105.

Lim EP, Tan CH, Jay TM, Dawe GS(2010). Locus coeruleus stimulation and noradrenergic modulation of hippocampal-prefrontal cortex long-term potentiation. Int J Neuropsychopharmacol 13:1219–1231.

Lindvall O, Björklund A. The organization of the ascending catecholamine neuron systems in the rat brain as revealed by the glyoxylic acid fluorescence method. Acta Physiol Scand Suppl. 1974;412:1-48.

Lippiello P, Hoxha E, Volpicelli F, Lo Duca G, Tempia F, Miniaci MC (2015). Noradrenergic modulation of the parallel fiber-Purkinje cell synapse in mouse cerebellum. Neuropharmacology 89:33–42.

Locus coeruleus phasic discharge is essential for stimulus-induced gamma oscillations in the prefrontal cortex. Ricardo M. Neves, Silvia van Keulen,

Mingyu Yang, Nikos K. Logothetis, and Oxana Eschenko. Journal of Neurophysiology 2018 119:3, 904-920.

Loughlin SE, Foote SL, Bloom FE. Efferent projections of nucleus locus coeruleus: topographic organization of cells of origin demonstrated by three-dimensional reconstruction. Neuroscience. 1986 Jun;18(2):291-306.

Marzo, A., Totah, N.K., Neves, R.M., Logothetis, N.K., Eschenko, O., 2014. Unilateral electrical stimulation of rat locus coeruleus elicits bilateral response of norepinephrine neurons and sustained activation of medial prefrontal cortex. J. Neurophysiol. 111 (12), 2570–2588.

Mather M, Clewett D, Sakaki M, Harley CW. Norepinephrine ignites local hotspots of neuronal excitation: How arousal amplifies selectivity in perception and memory. Behav Brain Sci. 2016 Jan;39:e200.

Mathis, A., Mamidanna, P., Cury, K.M. et al. DeepLabCut: markerless pose estimation of user-defined body parts with deep learning. Nat Neurosci 21, 1281–1289 (2018).

McCall, J. G., McCall, L. M., Harris, A. P., McKenna, J. T., Shukla, C., Strecker, R. E.,& McCoy, J. G. (2022). Role of the locus coeruleus and basal forebrain in arousal and attention. Brain Research Bulletin, 188, 47–58.

Muslimovic D, Post B, Speelman J D.et al Cognitive profile of patients with newly diagnosed Parkinson disease. Neurology 2005651239–1245

Özçete, Ö.D., Banerjee, A. & Kaeser, P.S. Mechanisms of neuromodulatory volume transmission. Mol Psychiatry 29, 3680–3693 (2024).

Pammer C, Gorcs T, Palkovits M (1990). Peptidergic innervation of the locus coeruleus cells in the human brain. Brain Res 515:247–255

Pickel VM, Segal M, Bloom FE. A radioautographic study of the efferent pathways of the nucleus locus coeruleus. J Comp Neurol. 1974 May 1;155(1):15–42.

Robertson, S. D., Plummer, N. W., de Marchena, J., & Jensen, P.(2013). Developmental origins of central norepinephrine neuron diversity. Nature Neuroscience, 16(8), 1016–1023.

Sara SJ. The locus coeruleus and noradrenergic modulation of cognition. Nat Rev Neurosci. 2009 Mar;10(3):211-23.

Sharpe M H. Auditory attention in early Parkinson's disease: an impairment in focused attention. Neuropsychologia 1992, 30101–106. [0.2cm] Slater, C.; Liu, Y.; Weiss, E.; Yu, K.; Wang, Q. The Neuromodulatory Role of the Noradrenergic and Cholinergic Systems and Their Interplay in Cognitive

Functions: A Focused Review. Brain Sci. 2022, 12, 890.

The International Brain Laboratory et al. A standardized and reproducible method to measure decision-making in mice. eLife 10, e63711 (2021).

Westlund KN, Coulter JD (1980). Descending projections of the locus coeruleus and subcoeruleus/medial parabrachial nuclei in monkey: axonal transport studies and dopamine-beta-hydroxylase immunocytochemistry. Brain Res 2:235–264.

Yu, A.J., & Dayan, P. (2002). Expected and Unexpected Uncertainty: ACh and NE in the Neocortex. Neural Information Processing Systems.

Zaborszky, L. The modular organization of brain systems. Basal forebrain: The last frontier. In Progress in Brain Research; Elsevier: Amsterdam, The Netherlands, 2002; Volume 136, pp. 359–372.

Appendix A

Additional data

Mouse	Bias	Threshold	High lapse rate	Low lapse rate
TH-cre Mo1	-3.4	0.57	0.36	0.1
TH-cre Mo2	-3.13	0.67	0.36	0.49
TH-cre Mo3	-32.69	32.13	0.24	0.37
DBH-cre x hTyr x Ai9 Mo4	12.03	1.13	0.58	0.06

Table A.1: Inferred psychometric curve parameters for each mouse (data pooled across all trials throughout learning)

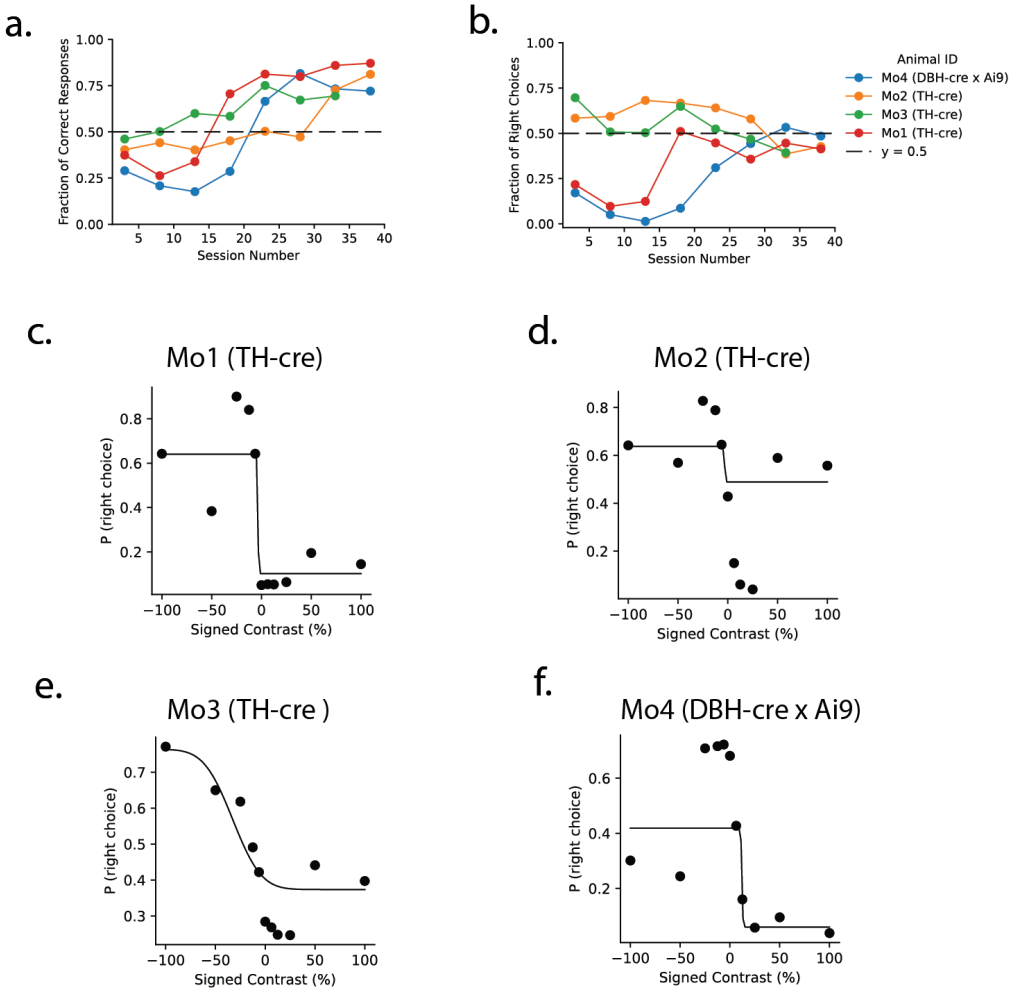

Figure A.1: Behaviour during task throughout learning trajectory for individual mice (n = 4 mice); **a.** Accuracy across learning trajectory. Each point represents average accuracy per 5 trials; **b.** Fraction of rightward choices across learning trajectory. Each point represents average accuracy per 5 trials; **c., d., e., f.** Psychometric curve for each mouse (data pooled across all trials throughout learning).

Trial type	TH-cre Mo1	TH-cre Mo2	TH-cre Mo3	DBH-cre x hTyr x Ai9 Mo4
Correct	2763	2177	1246	2282
Incorrect	608	426	543	769
Right	1264	1122	646	1282
Left	2107	1481	1143	1769
State 1	2400	1668	830	1934
State 2	786	756	667	694
State 3	185	180	292	424

Table A.2: Distribution of trials from each mouse included in population data (after learning)

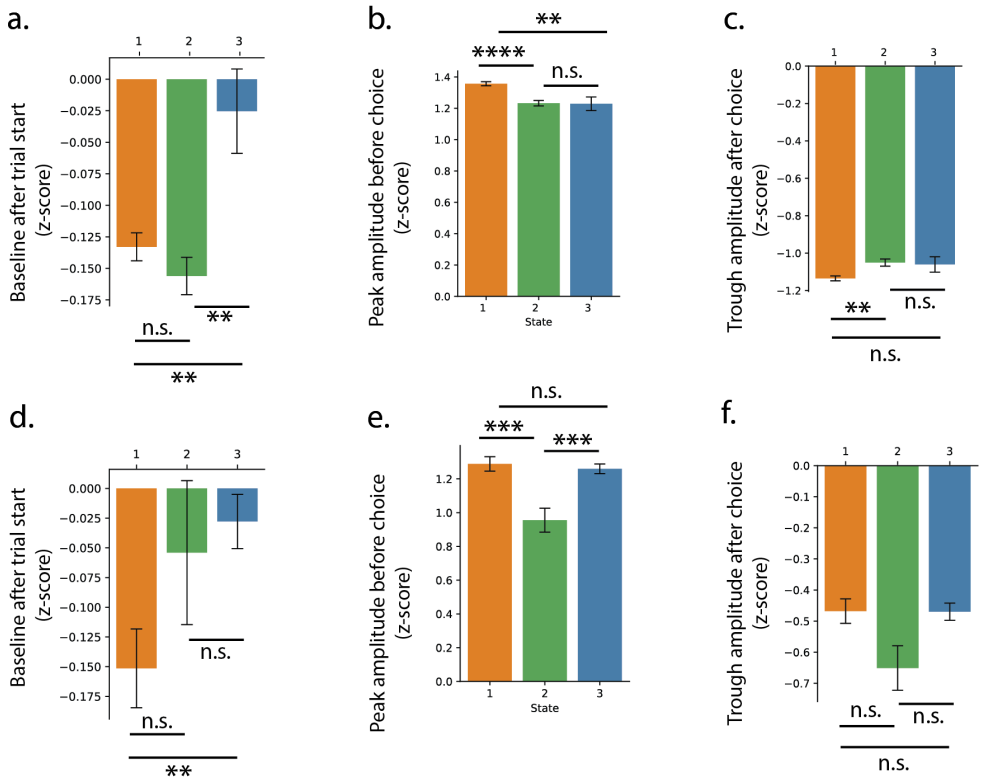

Figure A.2: LC neural dynamics during attentional states with respect to the outcome of the trial. **a.** Average baseline within 500 ms after a trial starts for all correct trials (error bars: SEM). One-way ANOVA with Bonferroni correction for pairwise comparisons: ANOVA F-statistic = 15.90535866, p-value $\leq$ 0.0001; **b.** Average peak amplitude within 500 ms before a choice is registered for all correct trials (error bars: SEM). One-way ANOVA with Bonferroni correction: ANOVA F-statistic = 21.59908885, p-value $\leq$ 0.0001; **c.** Average trough amplitude within 500 ms after a choice is registered for all correct trials (error bars: SEM). One-way ANOVA with Bonferroni correction: ANOVA F-statistic = 21.59908885, p-value $\leq$ 0.0001; **d.** Average baseline within 500 ms after a trial starts for all incorrect trials (error bars: SEM). One-way ANOVA with Bonferroni correction for pairwise comparisons: ANOVA F-statistic = 4.77796474, p-value = 0.008; **d.** Average peak amplitude within 500 ms before a choice is registered for all incorrect trials (error bars: SEM). One-way ANOVA with Bonferroni correction: ANOVA F-statistic = 8.257116733, p-value =0.0002; **f.** Average trough amplitude within 500 ms after a choice is registered for all incorrect trials (error bars: SEM). One-way ANOVA with Bonferroni correction: ANOVA F-statistic = 2.898645823, p-value is not significant. All Bonferroni corrected p-values are marked on the graph.